PAPER

Generalised ballooning theory of two-dimensional tokamak modes

IOP Publishing Plasma Physics and Controlled Fusion
Plasma Phys. Control. Fusion **60** (2018) 025011 (12pp) https://doi.org/10.1088/1361-6587/aa9352

Generalised ballooning theory of two-dimensional tokamak modes

P A Abdoul[1,2,3], D Dickinson[3], C M Roach[4] and H R Wilson[3]

[1] Charmo University, College of Education, Department of Physics, 46023 Chamchamal/Al-Sulaimaniyah, Kurdistan region, Iraq
[2] University of Sulaimani, College of Science, Department of Physics, 46001 Al-Sulaimaniyah, Kurdistan region, Iraq
[3] York Plasma Institute, Department of Physics, University of York, Heslington, York, YO10 5DD, United Kingdom
[4] CCFE, Culham Science Centre, Abingdon, Oxforshire, OX14 3DB, United Kingdom

E-mail: peshwaz.abdoul@charmouniversity.org

Received 4 August 2017, revised 2 October 2017
Accepted for publication 13 October 2017
Published 15 December 2017

Abstract

In this work, using solutions from a local gyrokinetic flux-tube code combined with higher order ballooning theory, a new analytical approach is developed to reconstruct the global linear mode structure with associated global mode frequency. In addition to the isolated mode (IM), which usually peaks on the outboard mid-plane, the higher order ballooning theory has also captured other types of less unstable global modes: (a) the weakly asymmetric ballooning theory (WABT) predicts a mixed mode (MM) that undergoes a small poloidal shift away from the outboard mid-plane, (b) a relatively more stable general mode (GM) balloons on the top (or bottom) of the tokamak plasma. In this paper, an analytic approach is developed to combine these disconnected analytical limits into a single generalised ballooning theory. This is used to investigate how an IM behaves under the effect of sheared toroidal flow. For small values of flow an IM initially converts into a MM where the results of WABT are recaptured, and eventually, as the flow increases, the mode asymptotically becomes a GM on the top (or bottom) of the plasma. This may be an ingredient in models for understanding why in some experimental scenarios, instead of large edge localised modes (ELMs), small ELMs are observed. Finally, our theory can have other important consequences, especially for calculations involving Reynolds stress driven intrinsic rotation through the radial asymmetry in the global mode structures. Understanding the intrinsic rotation is significant because external torque in a plasma the size of ITER is expected to be relatively low.

Keywords: generalised ballooning theory, local and global gyrokinetic codes, radial symmetry breaking

(Some figures may appear in colour only in the online journal)

1. Introduction

Cross-field turbulent transport of both heat and particles, widely believed to be caused by low frequency micro-instabilities is a main obstacle to achieving ignition in magnetically confined plasmas [1]. Hence, it is crucial to understand them and find a way to reduce their effects. Among the most interesting subject in this area, is the impact of global effects, such as plasma profile variations [2–4]. In this work, we focus on axisymmetric tokamaks in which the spatial component of the linearised gyrokinetic equations describing microinstabilities can be reduced to a 2D eigenmode equation in radius, x, and poloidal angle, θ. There are two main numerical treatments of the linear gyrokinetic equations, namely global and local, as we now discuss.

A global solution takes into account the effect of the radial profile variations, involving full solutions to the 2D eigenmode equations, providing both the global mode structure and associated global mode frequency. By contrast, the local approach employs a so-called ballooning theory to

reduce the problem to a 1D local system [5–8]. Moreover, ballooning theory has proven to be a powerful tool to investigate high toroidal mode number, $n \gg 1$, instabilities in tokamak plasmas. For this type of mode the distance between two neighbouring rational surfaces is negligible compared to the equilibrium scale length. Therefore, one can take advantage of this scale separation and employ the WKB treatment in a perturbation expansion. The lowest order in $1/n$, equivalent to local ballooning theory, exploits a so-called translation (or ballooning) symmetry, i.e the rational surfaces associated with an instability approximately experience the same equilibrium parameters as $n \to \infty$. This theory provides both local mode structures along field lines and the associated local complex mode frequency [5]. However, proceeding to the next order in the expansion breaks the translational symmetry, providing constraints to the local solutions, which determine the 2D global mode structures and their global mode frequency [5, 9–12]. In this paper, in the context of the higher order 'ballooning formalism', a new analytical theory is presented to reconstruct the 2D mode structures and calculate their mode frequencies from solutions to the local 1D ballooning equations. There are two main advantages of using local results to build up global mode structures; (a) they are computationally less intensive compared to full global solutions and (b) we can gain a deeper understanding of the physics behind the global mode structures [2, 13, 14].

The global mode structure can be reconstructed purely from the solutions to the local ballooning equations using the Fourier-ballooning representation [15]:

$$\tilde{\phi}(x,\,\theta) = \int_{-\infty}^{+\infty} \xi(x,\,\theta_0,\,\theta)\exp\left[-\mathrm{i}nq_0\theta\right] \times \exp\left[-\mathrm{i}nq'x(\theta-\theta_0)\right]Y(\theta_0)\mathrm{d}\theta_0. \quad (1)$$

Here, $\tilde{\phi}(x,\,\theta)$ is the global mode. The function $\xi(x,\,\theta_0,\,\theta)$ represents the local mode structure, and it is invariant under the double transformation $\theta_0 \to \theta_0 + 2\pi N$ and $\theta \to \theta + 2\pi N$ for integer N. The poloidal angle θ measures the distance along the magnetic field, n is the toroidal mode number and q_0 and $q' = \mathrm{d}q/\mathrm{d}x$ are the value of safety factor and its derivative on a rational surface at $x = 0$, respectively. The radial distance from a reference rational surface, $x = (r - r_s)/a$, is normalised to the tokamak minor radius a. It is assumed that the envelope $Y(\theta_0)$ varies much more rapidly than the local mode structure $\xi(\theta_0)$ with θ_0 (i.e $\frac{\mathrm{d}Y(\theta_0)}{\mathrm{d}\theta_0} \gg \frac{\mathrm{d}\xi(\theta_0)}{\mathrm{d}\theta_0}$) and satisfies the following differential equation [2]:

$$\frac{\lambda_{xx}(0,\,\theta_0)}{2n^2q'^2}\frac{\mathrm{d}^2Y(\theta_0)}{\mathrm{d}\theta_0^2} - \frac{\mathrm{i}\lambda_x(0,\,\theta_0)}{nq'}\frac{\mathrm{d}Y(\theta_0)}{\mathrm{d}\theta_0} + \left[\Omega - \lambda(0,\,\theta_0)\right]Y(\theta_0) = 0, \quad (2)$$

where, the periodic functions $\lambda(0,\,\theta_0)$, $\lambda_x(0,\,\theta_0)$ and $\lambda_{xx}(0,\,\theta_0)$ are obtained from the Taylor series expansion of the local complex mode frequency $\lambda(x,\,\theta_0) = \lambda_r(x,\,\theta_0) + \mathrm{i}\lambda_i(x,\,\theta_0)$ about $x = 0$ (λ_x and λ_{xx} denote the first and second derivative with respect to x). Here, the real $\lambda_r(x,\,\theta_0)$ and imaginary $\lambda_i(0,\,\theta_0)$ components correspond to the local frequency and local growth rate, respectively and $\Omega = \omega + \mathrm{i}\gamma$ is the global complex mode frequency with ω and γ being the global real frequency and growth rate. Note that, the periodicity constraint on $\tilde{\phi}(x,\,\theta)$ with θ requires a periodic $Y(\theta_0)$ in θ_0. Having knowledge of $Y(\theta_0)$ and its eigenvalue Ω from equation (2), together with the local mode structure $\xi(x,\,\theta_0,\,\theta)$, obtained from the local gyrokinetic codes, one may reconstruct the 2D mode structure, $\tilde{\phi}(x,\,\theta)$, from equation (1).

Providing a full analytic solution for equation (2) is quite challenging, but it has been solved in a few limits [5, 9–12, 16]; assuming $\lambda_x(0,\,\theta_0) = 0$, corresponding to a special case where $\lambda(x,\,\theta_0)$ has a stationary point at $x = 0$, leads to a highly unstable isolated mode (IM) that, for the poloidally up–down symmetric plasma equilibrium typically sits on the outboard mid-plane with global growth rate γ obtained from $\Omega = \lambda(x = 0,\,\theta_0 = 0) + O(1/n)$. However, when $\lambda_x(0,\,\theta_0) \neq 0$ and the second term in equation (2) dominates the first term involving $\lambda_{xx}(0,\,\theta_0)$, then the latter term can be neglected and one finds a relatively less unstable general mode (GM) that balloons on the top or bottom of the tokamak plasma. Its global growth rate and frequency involves an average over a period of θ_0, for instance see equation (46) (specifically $\Omega = \oint[\lambda(0,\,\theta_0)]\mathrm{d}\theta_0$). On the other hand, the weakly asymmetric ballooning theory (or WABT) expands equation (2) about $\theta_0 = 0$ and, by retaining up to the second order term in the expansion, leads to a mixed mode (MM), that slightly shifts with respect to the outboard mid-plane [13, 16][5]. More usually in realistic experimental situations, the global modes can sit anywhere in the poloidal plane [2, 3]. Therefore, to account for these modes, we have presented a new analytical theory that combines all the aforementioned analytical solutions into a single theory, namely a generalised ballooning theory (GBT). Specifically we can capture the sudden transition of an IM, through MM, into a GM as equilibrium profiles, such as the flow shear, evolve. This inter-mode transition has been considered as the basis for a model that could be used to understand the mechanism that underlies some classes of small ELMs [12, 17] and, hence, our theory can provide additional physical insights into these models.

Furthermore, it is worth mentioning that $\lambda_x(0,\,\theta_0)$ incorporates the effect of profile shearing, a special case of which is the rotational flow shear corresponding to $[\lambda_x(0,\,\theta_0)]_i = 0$, but $[\lambda_x(0,\,\theta_0)]_r \neq 0$, where the subscripts r and i correspond to the real and imaginary components, respectively. Flow shear can suppress the microinstabilities, thereby improving the plasma confinement [18–23]. However, it has recently been demonstrated that, in the presence of profile variations, flow shear can also destabilise the global instability such that for a critical value of flow shear, where the flow precisely compensates the effect of the profile variations, a highly unstable IM is captured [2, 4]. Finally, our theory has revealed that any poloidal shifts away from the outboard mid-plane are always accompanied by an

[5] Note that WABT in [13] takes into account the variation of $\lambda_x(0,\,\theta_0)$ and $\lambda_{xx}(0,\,\theta_0)$ with θ_0. While [16] is limited to a special case where the weakly θ_0-dependent part of $\lambda_x(0,\,\theta_0)$ and $\lambda_{xx}(0,\,\theta_0)$ are neglected. This simplification reduces equation (2) to the well known Weber equation which is exactly solved in terms of Hermite polynomials.

asymmetry in the radial eigenmode structure[6]. We found that the complex 'tilting angle', θ_b in our notation, serves as an important parameter accounting for radial symmetry breaking. The effect of complex 'tilting angle' is also discussed in [26] for the local and global analysing of the symmetry breaking of the 2D structure of the ITG modes. In addition, the radial asymmetry can generate a so-called Reynolds stress [11, 24, 25], which is very important, especially in calculations that employ quasilinear theory to model intrinsic rotation arising from Reynolds stress. Intrinsic rotation may be beneficial for a machine like ITER for which external momentum sources are weak or not practical. In such theories Reynolds stress can, in principle, contribute to the generation of poloidal flows in the edge region of tokamak plasmas during the low to high mode transition [27, 28].

This paper is organised as follows. Section 2 is devoted to solving equations (1) and (2) analytically. In this section, we have applied our theory to explain and understand the radial asymmetry associated with a mode that undergoes a poloidal shift with respect to the outboard mid-plane. In section 3 we have validated our theory by recapturing an IM, MM and GM in special limits. In section 4, using available data from the literature for a toroidal ion temperature gradient (ITG) model in a large aspect ratio circular tokamaks, we have benchmarked our calculations against numerical solutions. Finally, the conclusion and future plans are presented in section 5.

2. Generalised ballooning theory

In this section, we develop a new analytical approach that combines all previously obtained analytical solutions for IMs, MMs and GMs into a single GBT.

2.1. The envelope $Y(\theta_0)$ and Ω

We start with equation (2) and seek localised solutions with a form:

$$Y(\theta_0) = \exp\left[-nq'F(\theta_0)\right], \tag{3}$$

where $F(\theta_0)$ is a 2π periodic function of θ_0. In this paper, assuming $nq' \gg 1$, we shall generalise the restricted solutions of WABT by expanding about $\theta_0 = \theta_b$ rather than $\theta_0 = 0$. At this point θ_b is arbitrary but in the following we shall describe the procedure to determine its value. We now Taylor expand about $\theta_0 = \theta_b$, retaining up to the second order terms in $\theta_0 - \theta_b$, and write[7]

$$Y(\theta_0) \approx \exp\left[-nq'\alpha(\theta_0 - \theta_b)^2\right] \tag{4}$$

$$\begin{aligned}
\lambda_{xx}(0, \theta_0) &\approx \lambda_{xx}(0, \theta_b) + \lambda_{xx\theta_0}(0, \theta_b)(\theta_0 - \theta_b) \\
&\quad + \frac{\lambda_{xx\theta_0\theta_0}(0, \theta_b)}{2}(\theta_0 - \theta_b)^2 \\
\lambda_x(0, \theta_0) &\approx \lambda_x(0, \theta_b) + \lambda_{x\theta_0}(0, \theta_b)(\theta_0 - \theta_b) \\
&\quad + \frac{\lambda_{x\theta_0\theta_0}(0, \theta_b)}{2}(\theta_0 - \theta_b)^2 \\
\lambda(0, \theta_0) &\approx \lambda(0, \theta_b) + \lambda_{\theta_0}(0, \theta_b)(\theta_0 - \theta_b) \\
&\quad + \frac{\lambda_{\theta_0\theta_0}(0, \theta_b)}{2}(\theta_0 - \theta_b)^2,
\end{aligned} \tag{5}$$

where, the subscripts θ_0 and $\theta_0\theta_0$ on F and the coefficients λ, λ_x and λ_{xx} refer, respectively, to their first and second derivatives with respect to θ_0 and are evaluated at $\theta_0 = \theta_b$. Here we have absorbed constant factors into $Y(\theta_0)$ and $F_{\theta_0\theta_0}(\theta_b)$ is replaced by 2α. In addition, we define θ_b as the location of maximum $F(\theta_0)$, so that $F_{\theta_0}(\theta_b) = 0$. After substituting equations (4) and (5) back into equation (2), and equating coefficients with like powers of $(\theta_0 - \theta_b)$, we obtain the following equation for α:

$$\begin{aligned}
\alpha = &\frac{\lambda_{xx\theta_0\theta_0}(0, \theta_b)}{8nq'\lambda_{xx}(0, \theta_b)} - \frac{\mathrm{i}\lambda_{x\theta_0}(0, \theta_b)}{2\lambda_{xx}(0, \theta_b)} \\
&+ \delta\left[\left(\frac{\lambda_{xx\theta_0\theta_0}(0, \theta_b)}{8nq'\lambda_{xx}(0, \theta_b)} - \frac{\mathrm{i}\lambda_{x\theta_0}(0, \theta_b)}{2\lambda_{xx}(0, \theta_b)}\right)^2\right. \\
&\left. + \frac{\lambda_{\theta_0\theta_0}(0, \theta_b)}{4\lambda_{xx}}\right]^{1/2},
\end{aligned} \tag{6}$$

an equation to be solved for θ_b

$$\left[2\mathrm{i}\lambda_x(0, \theta_b) - \frac{\lambda_{xx\theta_0}(0, \theta_b)}{nq'}\right]\alpha = \lambda_{\theta_0}(0, \theta_b), \tag{7}$$

and the following solution for Ω:

$$\Omega = \lambda(0, \theta_b) + \left[\frac{\lambda_{xx}(0, \theta_b)}{nq'}\right]\alpha, \tag{8}$$

where $\delta = \pm 1$ and the sign is chosen such that $Y(\theta_0)$ is localised in θ_0 space. Finally, these results can be combined to derive the following form for $Y(\theta_0)$

$$\begin{aligned}
Y(\theta_0) = &\exp\left[-nq'\alpha(\theta_0 - \theta_m)^2\right] \\
&\times \exp\left[\left(\frac{2inq'|\alpha|^2}{\alpha_r}\theta_{bi}\right)\theta_0\right],
\end{aligned} \tag{9}$$

where, constant factors are absorbed into $Y(\theta_0)$ and the subscripts r and i corresponding to the real and imaginary parts, respectively. The real parameter,

$$\theta_m = \theta_{br} - \frac{\alpha_i}{\alpha_r}\theta_{bi} \tag{10}$$

determines where the magnitude of $Y(\theta_0)$ peaks in θ_0 space[8]. Furthermore, the last exponential term on the right-hand side of equation (9) controls the symmetry of $|Y(\theta_0)|$ about a line that goes through $\theta_0 = \theta_m$. We note that the resultant $Y(\theta_0)$ is symmetric about $\theta_0 = \theta_m$ only for a set of equilibrium

[6] Note that, by taking the radial slice from the constructed mode structure at $\theta = 0$, the radial asymmetry is measured with respect to a rational surface about which the mode peaks.

[7] It is worth mentioning that we are evaluating $Y(\theta_0)$ only for real θ_0 but the parameter θ_b can be, in general, complex. The imaginary component of θ_b is related to the symmetry of $Y(\theta_0)$ which, in turn, as we shall see in 2.2, causes a radial shift of the mode off $x = 0$.

[8] Note that, θ_m also determines the mode physical poloidal position with respect to the outboard mid-plane.

parameters that provides $\theta_{bi} = 0$, corresponding to $\theta_m = \theta_{br}$ in equation (10). This symmetry breaking has important consequences for the reconstructed global mode structure, as we now turn to discuss in the following subsection.

2.2. The global mode structure $\tilde{\phi}(x, \theta)$

Now to calculate the global eigenmode structures, we substitute $Y(\theta_0)$ from equation (4) into the Fourier ballooning representation in equation (1), and assuming that $\xi(x, \theta, \theta_0)$ varies slowly with θ_0 compared to $Y(\theta_0)$, we can then apply the stationary phase approximation to the integral in equation (1). To lowest order we find:

$$\begin{aligned}\tilde{\phi}(x, \theta) \approx\ & \xi(x, \theta_m, \theta)\exp\left[-nq'\alpha\theta_b^2\right]\exp\left[-inq_0\theta\right] \\ & \times \exp\left[-inq'\theta x - \frac{nq'}{4\alpha}(x - 2i\alpha\theta_b)^2\right] \\ & \times \int_{-\infty}^{+\infty} \exp\left[-nq'\alpha\left(\theta_0 - \left(\theta_b + \frac{ix}{2\alpha}\right)\right)^2\right]d\theta_0,\end{aligned} \tag{11}$$

where θ_m is defined in equation (10). The integration on the right-hand side of equation (11) is a well known Gaussian with a complex shift $\theta_b + \frac{ix}{2\alpha}$ and the result is $\sqrt{\frac{\pi}{nq'\alpha}}$ [29, 30]. To determine the mode physical radial shift and investigate its radial symmetry we shall first decompose α and θ_b into their real and imaginary components to obtain

$$\begin{aligned}\tilde{\phi}(x, \theta) \approx\ & \sqrt{\frac{\pi}{nq'\alpha}}\,\xi(x, \theta_m, \theta)\exp\left[-inq_0\theta\right] \\ & \times \exp\left[-inq'\theta x\right]\exp\left[-\frac{nq'\alpha_r}{4|\alpha|^2}(x^2 - 2x_m x)\right] \\ & \times \exp\left[\frac{inq'\alpha_i}{4|\alpha|^2}(x^2 - 2x_m x)\right]\exp\left[inq'\theta_m x\right].\end{aligned} \tag{12}$$

Now by completing the square in x then rearrange the terms in equation (12) we get

$$\begin{aligned}\tilde{\phi}(x, \theta) \approx\ & \xi(x, \theta_m, \theta)\exp\left[-inq_0\theta\right] \\ & \times \exp\left[-\frac{nq'}{4\alpha}(x - x_m)^2\right] \\ & \times \exp\left[-inq'(\theta - \theta_m)x\right],\end{aligned} \tag{13}$$

where, again we have absorbed constant factors into $\tilde{\phi}(x, \theta)$. Here, the real parameter,

$$x_m = -\frac{2\,|\alpha|^2}{\alpha_r}\theta_{bi} \tag{14}$$

represents a physical radial shift away from $x = 0$. From equations (13) and (14) it is clear that if $\theta_{bi} \neq 0$, corresponding to asymmetric $Y(\theta_0)$ about $\theta_0 = \theta_m$ in equation (9), the reconstructed global mode, in turn, undergoes a radial shift away from its associated rational surface at $x = 0$. Furthermore, from the last exponential on the right side of equation (13), we can see that $\tilde{\phi}(x, \theta)$ has a radial symmetry about $x = x_m$ only when $\theta = \theta_m$. However, if we take the radial slice from the constructed mode structure at $\theta = 0$, only IMs, for which $\theta = \theta_m = 0$, have radial symmetry. Thus, we conclude that; any poloidal shift with respect to $\theta = 0$ introduces asymmetry into the radial mode structures.

Finally, the mode's radial width is determined from the full width at half maximum (FWHM) of the Gaussian (second exponential term on the right-hand side in equation (13)), which reads

$$\Delta_x = \frac{4\sqrt{\log(2)}\,|\alpha|}{\sqrt{n|q'|}\,\sqrt{|\alpha_r|}}. \tag{15}$$

3. Validation of GBT

The core purpose of this section is to test some of the key predictions of our new theory by reproducing analytical results for all IMs, MMs and GMs that have been previously derived in [9–11, 16] for instance. We note that, to obtain theses modes, a few simplifications and assumptions are made in literature. Hence, to recapture those solutions from our GBT theory, we shall employ similar simplifications. Firstly, we neglect the weak θ_0-dependence of both $\lambda_x(0, \theta_0)$ and $\lambda_{xx}(0, \theta_0)$ and write

$$\begin{aligned}\lambda_x(0, \theta_0) &= \lambda_x \\ \lambda_{xx}(0, \theta_0) &= \lambda_{xx},\end{aligned} \tag{16}$$

where λ_x and λ_{xx} are, in general, complex numbers. Moreover, knowing the fact that $\lambda(0, \theta_0)$ is periodic in θ_0 we may Fourier expand to obtain

$$\lambda(0, \theta_0) = \lambda_0 + \lambda_1\cos(\theta_0), \tag{17}$$

where, only two Fourier harmonics have been retained. For this simplified model equation (6) reduces to

$$\alpha = \frac{i\delta}{2}\sqrt{\frac{\lambda_1}{\lambda_{xx}}\cos(\theta_b)}. \tag{18}$$

This, in turn, simplifies both $Y(\theta_0)$ in equation (4) and Ω in equation (8):

$$Y(\theta_0) = \exp\left[\frac{-inq'\delta}{2}\sqrt{\frac{\lambda_1}{\lambda_{xx}}\cos(\theta_b)}\,(\theta_0 - \theta_b)^2\right] \tag{19}$$

and

$$\Omega = \lambda_0 + \lambda_1\cos(\theta_b) + \frac{i\lambda_{xx}\delta}{2nq'}\sqrt{\frac{\lambda_1}{\lambda_{xx}}\cos(\theta_b)}. \tag{20}$$

Furthermore, the corresponding global mode structure $\tilde{\phi}(x, \theta)$ (from equation (13)) with its radial mode width (equation (15)) are, respectively, reduced to

$$\begin{aligned}\tilde{\phi}(x, \theta) \sim\ & \xi(x, \theta_m, \theta)\exp\left[-inq_0\theta\right] \\ & \times \exp\left[\frac{inq'\delta}{2\sqrt{\frac{\lambda_1}{\lambda_{xx}}\cos(\theta_b)}}(x - x_m)^2\right] \\ & \times \exp\left[-inq'(\theta - \theta_m)x\right]\end{aligned} \tag{21}$$

and

$$\Delta_x = \frac{2\sqrt{2\log(2)}}{\sqrt{n|q'|}} \frac{\left|\sqrt{\frac{\lambda_1}{\lambda_{xx}}\cos(\theta_b)}\right|}{\sqrt{\left|\left[\sqrt{\frac{\lambda_1}{\lambda_{xx}}\cos(\theta_b)}\right]_i\right|}}, \tag{22}$$

where, both θ_m (from equation (10)) and x_m (from equation (14)), respectively, take the following forms

$$\theta_m = \theta_{br} + \frac{\left[\sqrt{\frac{\lambda_1}{\lambda_{xx}}\cos(\theta_b)}\right]_r}{\left[\sqrt{\frac{\lambda_1}{\lambda_{xx}}\cos(\theta_b)}\right]_i} \times \theta_{bi}, \tag{23}$$

$$x_m = \delta \frac{\left|\sqrt{\frac{\lambda_1}{\lambda_{xx}}\cos(\theta_b)}\right|^2}{\left[\sqrt{\frac{\lambda_1}{\lambda_{xx}}\cos(\theta_b)}\right]_i} \times \theta_{bi}. \tag{24}$$

Now, to calculate θ_b, we substitute equations (16) and (17) into equation (7) and rearrange to obtain

$$\cos^2(\theta_b) + \left(\left|\frac{\lambda_x^2}{\lambda_1\lambda_{xx}}\right| \exp\left[\mathrm{i}\arg\left(\frac{\lambda_x^2}{\lambda_1\lambda_{xx}}\right)\right]\right) \times \cos(\theta_b) - 1 = 0, \tag{25}$$

where, we have expressed the complex number $\lambda_x^2/\lambda_1\lambda_{xx}$ in polar form to write

$$\frac{\lambda_x^2}{\lambda_1\lambda_{xx}} = \left|\frac{\lambda_x^2}{\lambda_1\lambda_{xx}}\right| \exp\left[\mathrm{i}\arg\left(\frac{\lambda_x^2}{\lambda_1\lambda_{xx}}\right)\right] \tag{26}$$

and equation (25) is written in a form such that the real parameter $|\lambda_x^2/\lambda_1\lambda_{xx}|$ is used in the subsequent subsections to solve equation (25) perturbativley to reproduce the analytical solutions for IMs, MMs and GMs, respectively. Here, $|\lambda_x^2/\lambda_1\lambda_{xx}|$ and $\arg(\lambda_x^2/\lambda_1\lambda_{xx})$ refer to the magnitude and argument of $\lambda_x^2/\lambda_1\lambda_{xx}$, respectively.

3.1. Isolated modes: $\lambda_x = 0$

We start by substituting $\lambda_x = 0$ into equation (25) to obtain

$$\cos(\theta_b^{\pm}) = \pm 1, \tag{27}$$

where plus and minus signs has solutions $\theta_b^+ = 0$ and $\theta_b^- = \pm\pi$, respectively. Therefore, for both solutions $\theta_{bi} = 0$ which then provides a symmetric $Y(\theta_0)$ in equation (19) and from equation (23) we have $\theta_m^+ = \theta_{br}^+ = 0$ (or $\theta_m^- = \theta_{br}^- = \pm\pi$) leading to a mode that peaks on the outboard (or inboard) mid-plane and radially centred on $x = x_m^{\pm} = 0$. The corresponding analytical solutions, using the results given in section 3 (from equations (19) to (22)), are reduced to the following forms[9]

$$\begin{aligned} Y_I^+(\theta_0) &= \exp\left[-\frac{\mathrm{i}nq'\delta^+}{2}\sqrt{\frac{\lambda_1}{\lambda_{xx}}}(\theta_0)^2\right] \\ Y_I^-(\theta_0) &= \exp\left[\frac{nq'\delta^-}{2}\sqrt{\frac{\lambda_1}{\lambda_{xx}}}(\theta_0 \mp \pi)^2\right], \end{aligned} \tag{28}$$

$$\Omega_I^{\pm} = \lambda_0 \pm \lambda_1 + \frac{\mathrm{i}\delta^{\pm}\sqrt{\pm\lambda_1\lambda_{xx}}}{2nq'}, \tag{29}$$

$$\begin{aligned} \tilde{\phi}_I^+(x,\theta) &\sim \xi(x,\theta_m^+ = 0,\theta)\exp[-\mathrm{i}nq\theta] \\ &\quad \times \exp\left[\frac{\mathrm{i}nq'\delta^+}{2\sqrt{\frac{\lambda_1}{\lambda_{xx}}}}x^2\right] \\ \tilde{\phi}_I^-(x,\theta) &\sim \xi(x,\theta_m^- = \pm\pi,\theta)\exp[-\mathrm{i}nq\theta] \\ &\quad \times \exp\left[\frac{nq'\delta^-}{2\sqrt{\frac{\lambda_1}{\lambda_{xx}}}}x^2\right]\exp[\pm\mathrm{i}\pi nq'x], \end{aligned} \tag{30}$$

$$\Delta_{xI}^{\pm} = \frac{2\sqrt{2\log(2)}}{\sqrt{n|q'|}} \frac{|\sqrt{\pm\lambda_1/\lambda_{xx}}|}{\sqrt{|[\sqrt{\pm\lambda_1/\lambda_{xx}}]_i|}} \tag{31}$$

where $q = q_0 + q'x$ and the subscript 'I' refers to an IM. Furthermore, our equation (28) and equation (29) corresponding to $Y(\theta_0)$ and its eigenvalue Ω, respectively, are exactly equivalent to equations (4) and (5) in [12] (note that in [12] our coefficients λ_1 and λ_{xx} are replaced by $-\Omega_{\theta_0\theta_0}$ and Ω_{xx}, respectively). Hence, we conclude that the mode that sits in the bad curvature region at $\theta = 0$, corresponding to plus sign solutions, is an IM. However, the additional mode that has been captured on the good curvature region at $\theta = \pm\pi$, corresponding to minus sign solutions, we called an anti-IM. Moreover, for a real physical system we expect IMs to be more unstable than anti-IMs due to the stabilising influence of good curvature region. This, in turn, provides a constraint on the model coefficients. To see this, we may use equation (29) and define a controlling parameter $\Delta_{\Omega}^{\pm}$ such that $\Delta_{\Omega}^{\pm} = \Omega_I^+ - \Omega_I^-$; after neglecting small corrections arising from $O(1/n)$ terms we obtain $\Delta_{\Omega}^{\pm} \approx 2\lambda_1$. Note, therefore, that an IM can be more unstable than an anti-IM if and only if

$$[\Delta_{\Omega}^{\pm}]_i = 2[\lambda_1]_i > 0. \tag{32}$$

Here, subscript i refer to the imaginary component.

3.2. Mixed modes: $|\lambda_x^2/\lambda_1\lambda_{xx}| \ll 1$

In this subsection we focus on a MM that undergoes a small poloidal shift with respect to the outboard (or inboard) mid-plane. Here, we try to reproduce the so-called WABT of [13, 16] in the limit $|\lambda_x^2/\lambda_1\lambda_{xx}| \ll 1$. In this limit, treating $|\lambda_x^2/\lambda_1\lambda_{xx}|$ as our small parameter, we apply a so-called regular perturbation theory to solve equation (25) for $\cos(\theta_b)$ and to the first order we obtain

$$\cos(\theta_b^{\pm}) \approx \pm 1 - \frac{\lambda_x^2}{2\lambda_1\lambda_{xx}}, \tag{33}$$

[9] Note that $\delta^+ = \pm 1$ ($\delta^- = \pm 1$) and the sign is chosen such that the mode on outboard (inboard) mid-plane is localised about $\theta_0 = 0$ ($\theta_0 = \pm\pi$).

where the leading order solution of equation (33) is equivalent to equation (27) corresponding to IMs and anti-IMs. By expanding $\cos(\theta_b^+)$ and $\cos(\theta_b^-)$ in equation (33) about 0 and $\pm\pi$, respectively, and by retaining up to the second order terms in the expansion, equation (33) leads to the following solutions for θ_b^+ and θ_b^-

$$\theta_b^+ \approx \sqrt{\frac{\lambda_x^2}{\lambda_1\lambda_{xx}}} = \frac{\sigma^+\lambda_x}{\sqrt{\lambda_1\lambda_{xx}}} \tag{34}$$

and

$$\theta_b^- \approx \pm\pi + \sqrt{\frac{-\lambda_x^2}{\lambda_1\lambda_{xx}}} = \pm\pi + \frac{\sigma^-\mathrm{i}\lambda_x}{\sqrt{\lambda_1\lambda_{xx}}}, \tag{35}$$

where, sign of $\sigma^+ = \pm 1$ (or $\sigma^- = \pm 1$) controls the mode poloidal shift in the upward or downward direction with respect to the outboard (or inboard) mid-plane. Now the analytical solutions, using the results given in section 3 (from equations (19) to (24)), are reduced to the following forms[10]:

$$\begin{aligned} Y_M^+(\theta_0) &\approx \exp\left[-\frac{\mathrm{i}nq'\delta^+}{2}\sqrt{\frac{\lambda_1}{\lambda_{xx}}}\left(\theta_0 - \frac{\sigma^+\lambda_x}{\sqrt{\lambda_1\lambda_{xx}}}\right)^2\right] \\ Y_M^-(\theta_0) &\approx \exp\left[\frac{nq'\delta^-}{2}\sqrt{\frac{\lambda_1}{\lambda_{xx}}}\left(\theta_0 - \frac{\sigma^-\mathrm{i}\lambda_x}{\sqrt{\lambda_1\lambda_{xx}}} \mp \pi\right)^2\right], \end{aligned} \tag{36}$$

$$\Omega_M^\pm \approx \lambda_0 \pm \lambda_1 - \frac{\lambda_x^2}{2\lambda_{xx}} + \frac{\mathrm{i}\delta^\pm\sqrt{\pm\lambda_1\lambda_{xx}}}{2nq'}, \tag{37}$$

$$\begin{aligned} \tilde{\phi}_M^\pm(x,\theta) \sim\ & \xi(x,\theta_m^\pm,\theta)\exp[-\mathrm{i}nq_0\theta] \\ & \times \exp\left[\frac{\mathrm{i}nq'\delta^\pm\sqrt{\pm\lambda_{xx}/\lambda_1}}{2}(x - x_m^\pm)^2\right] \\ & \times \exp[-\mathrm{i}nq'(\theta - \theta_m^\pm)x], \end{aligned} \tag{38}$$

$$\Delta_{xM}^\pm \approx \frac{2\sqrt{2\log(2)}}{\sqrt{n|q'|}} \frac{\left|\sqrt{\frac{\pm\lambda_1}{\lambda_{xx}}}\right|}{\sqrt{\left|\left[\sqrt{\frac{\pm\lambda_1}{\lambda_{xx}}}\right]_i\right|}}, \tag{39}$$

$$\begin{aligned} \theta_{mM}^+ &\approx \left[\frac{\sigma^+\lambda_x}{\sqrt{\lambda_1\lambda_{xx}}}\right]_r + \frac{\left[\sqrt{\frac{\lambda_1}{\lambda_{xx}}}\right]_r\left[\frac{\sigma^+\lambda_x}{\sqrt{\lambda_1\lambda_{xx}}}\right]_i}{[\sqrt{\lambda_1/\lambda_{xx}}]_i} \\ \theta_{mM}^- &\approx \pm\pi - \left[\frac{\sigma^-\lambda_x}{\sqrt{\lambda_1\lambda_{xx}}}\right]_i - \frac{\left[\sqrt{\frac{\lambda_1}{\lambda_{xx}}}\right]_i\left[\frac{\sigma^-\lambda_x}{\sqrt{\lambda_1\lambda_{xx}}}\right]_r}{[\sqrt{\lambda_1/\lambda_{xx}}]_r}, \end{aligned} \tag{40}$$

$$\begin{aligned} x_{mM}^+ &\approx \delta^+ \frac{\left|\sqrt{\frac{\lambda_1}{\lambda_{xx}}}\right|^2\left[\frac{\sigma^+\lambda_x}{\sqrt{\lambda_1\lambda_{xx}}}\right]_i}{\left[\sqrt{\frac{\lambda_1}{\lambda_{xx}}}\right]_i} \\ x_{mM}^- &\approx \delta^- \frac{\left|\sqrt{\frac{\lambda_1}{\lambda_{xx}}}\right|^2\left[\frac{\sigma^-\lambda_x}{\sqrt{\lambda_1\lambda_{xx}}}\right]_r}{\left[\sqrt{\frac{\lambda_1}{\lambda_{xx}}}\right]_r}, \end{aligned} \tag{41}$$

where, the subscript '*M*' refers to a MM and for $\lambda_x = 0$ we recapture both IMs and anti-IMs of the previous subsection corresponding to θ_b^+ and θ_b^-, respectively. Finally, we note that equations (36)–(41) are exactly what we would have obtained if we have started with equation (2) by neglecting the weak θ_0-dependence of both $\lambda_{xx}(\theta_0)$ and $\lambda_x(\theta_0)$ and expanding about $\theta_0 = 0$ (or $\theta_0 = \pm\pi$) rather than $\theta_0 = \theta_b$. This is called a WABT which deals only with a MM that sits close to the outboard (or inboard) mid-plane [13, 16]. Note also that, according to WABT, the radial mode width (from equation (39)) is constant and does not depend on λ_x[11].

3.3. General modes: $|\lambda_x^2/\lambda_1\lambda_{xx}| \gg 1$

We start by applying a so-called singular perturbation theory to solve equation (25) for $|\lambda_x^2/\lambda_1\lambda_{xx}| \gg 1$ and obtain the following two solutions:

$$\cos(\sigma^+\theta_b^+) \approx +\frac{\lambda_1\lambda_{xx}}{\lambda_x^2} \tag{42}$$

and

$$\cos(\sigma^-\theta_b^-) \approx -\frac{\lambda_x^2}{\lambda_1\lambda_{xx}} \tag{43}$$

where equations (42) and (43) are both symmetric with respect to the sign of $\sigma^+ = \pm 1$ and $\sigma^- = \pm 1$, respectively. We shall first consider the 'θ_b^+' solution and after substituting $\cos(\sigma^+\theta_b^+)$ from equation (42) into equation (18) and equation (20), we obtain

$$\alpha_g^+ \approx \frac{\mathrm{i}\delta^+\lambda_1}{2\lambda_x} \tag{44}$$

and

$$\Omega_g^+ \approx \lambda_0 + \frac{\lambda_1^2\lambda_{xx}}{\lambda_x^2} + \frac{\mathrm{i}\delta^+\lambda_1\lambda_{xx}}{2nq'\lambda_x}, \tag{45}$$

respectively. Where, the subscript '*g*' refers to a GM. Note also that if we take the limit $|\lambda_x^2/\lambda_1\lambda_{xx}| \to \pm\infty$, from equation (42) we have $\cos(\theta_b^+) \to 0$. This leads to two solutions with $\theta_b^+ \to \sigma^+\pi/2$, where $\sigma^+ = \pm 1$, 'plus' and 'minus' signs correspond to a mode that asymptotically approaches the top and bottom of the tokamak plasma,

[10] Here, using the fact that $|\lambda_x^2/\lambda_1\lambda_{xx}| \ll 1$ we have only considered the dominant leading order term in calculating $\delta^\pm\sqrt{\frac{\lambda_1}{\lambda_{xx}}}\cos(\theta_b^\pm)$ from equation (33) and, hence, we have written $\delta^\pm\sqrt{\frac{\lambda_1}{\lambda_{xx}}}\cos(\theta_b^\pm) \approx \delta^\pm\sqrt{\pm\lambda_1/\lambda_{xx}}$.

[11] It is worth mentioning that in a parameter regime for which the condition $|\lambda_x^2/\lambda_1\lambda_{xx}| \ll 1$ breaks down, the radial mode width does indeed vary with λ_x. An example of this is a GM discussed in section 3.3 (for a more general case see section 4, specifically figure 1)

respectively. In this limit, from equation (45) we have[12]

$$\Omega_g^+ \approx \lambda_0. \tag{46}$$

This indicates that the mode has a similar eigenvalue as a GM that has been previously studied in the literature, see [9–11] for instance. However, this is necessary but not sufficient to see if they represent the same mode. Therefore, to check this we proceed further with our calculations and investigate the corresponding envelope $Y^+(\theta_0)$. Now using α_g^+ from equation (44) and after multiplying the right-hand side of equation (19) by a constant factor $\exp[inq'\sigma^+\delta^+\lambda_1/\lambda_x]$, we obtain the following formula for $Y^+(\theta_0)$

$$Y_g^+(\theta_0) \approx \exp\left[inq'\frac{\sigma^+\delta^+\lambda_1}{\lambda_x}\left(1-\frac{(\theta_0-\theta_b^+)^2}{2}\right)\right]. \tag{47}$$

Knowing that the limit $|\lambda_x^2/\lambda_1\lambda_{xx}| \to \pm\infty$ leads to $\theta_b^+ \to \sigma^+\pi/2$, the term $\sigma^+\left[1-\frac{(\theta_0-\theta_b^+)^2}{2}\right]$ in the exponent on right-hand side of equation (47), in turn, can be approximated by $\sigma^+\left[1-\frac{(\theta_0-(\sigma^+\pi/2))^2}{2}\right]$. This represents a Taylor series expansion of $\sin(\theta_0)$ about $\sigma^+\pi/2$ such that equation (47) is rewritten to get

$$Y_g^+(\theta_0) \approx \exp\left[inq'\frac{\delta^+\lambda_1}{\lambda_x}\sin(\theta_0)\right]. \tag{48}$$

This is similar to the eigenfunction of a GM that one obtains by solving a first order ODE after neglecting the coefficient associated with the second order derivative term in equation (2). Therefore, we have demonstrated that our GBT has captured a general like mode (GM) in the limit $|\lambda_x^2/\lambda_1\lambda_{xx}| \to \pm\infty$. Furthermore, because $\theta_{bi}^+ = 0$, corresponding to $x_m = 0$ in equation (24), we rewrite equation (21) to obtain the reconstructed global mode structure $\tilde{\phi}(x,\theta)$ for a GM which reads

$$\begin{aligned}\tilde{\phi}_g^+(x,\theta) \sim \xi\left(x,\theta_m^+ \approx \sigma^+\frac{\pi}{2},\theta\right)&\exp[-inq_0\theta]\\ &\times\exp\left[\frac{inq'\delta^+\lambda_x}{2\lambda_1}x^2\right]\\ &\times\exp\left[-inq'\left(\theta-\sigma^+\frac{\pi}{2}\right)x\right]\end{aligned} \tag{49}$$

and the corresponding mode radial width from equation (22) reduces to

$$\Delta_{xg}^+ \approx \frac{2\sqrt{2\log(2)}\,|\lambda_1/\lambda_x|}{\sqrt{n|q'|}\sqrt{|[\lambda_1/\lambda_x]_i|}}, \tag{50}$$

where, from equation (50), we note that the mode radial width is affected by λ_x, but, according to equation (46), its growth rate is unchanged.

[12] Note that we can write $\lambda_0 = \frac{1}{2\pi}\oint[\lambda(0,\theta_0)]\mathrm{d}\theta_0$, where from equation (17) we have $\lambda(0,\theta_0) = \lambda_0 + \lambda_1\cos(\theta_0)$ and $\frac{1}{2\pi}\oint[...]\mathrm{d}\theta_0$ refers to an average over a period in θ_0.

Finally, we investigate the 'θ_b^-' solution by decomposing equation (43) into its real and imaginary components to obtain

$$\begin{aligned}\cos(\sigma^-\theta_{br}^-)\cosh(\sigma^-\theta_{bi}^-) &\approx -\left[\frac{\lambda_x^2}{\lambda_1\lambda_{xx}}\right]_r\\ \sin(\sigma^-\theta_{br}^-)\sinh(\sigma^-\theta_{bi}^-) &\approx \left[\frac{\lambda_x^2}{\lambda_1\lambda_{xx}}\right]_i.\end{aligned} \tag{51}$$

We shall now square the real and imaginary parts in equation (51), replacing $\sinh^2(\sigma^-\theta_{bi}^-)$ by $\cosh^2(\sigma^-\theta_{bi}^-) - 1$, and add them to obtain $\cosh^2(\sigma^-\theta_{bi}^-) = \sin^2(\sigma^-\theta_{br}^-) + |\lambda_x^2/\lambda_1\lambda_{xx}|^2$. Knowing that $0 \leqslant \sin^2(\sigma^-\theta_{br}^-) \leqslant 1$ and due to the fact that $|\lambda_x^2/\lambda_1\lambda_{xx}| \gg 1$ we conclude that $\cosh\sigma^-\theta_{bi}^- \gg 1$. This indicates that $|\theta_{bi}^-| \gg 1$. The reconstructed global mode, in turn, undergoes a big radial shift away from the reference rational surface at $x = 0$ invalidating the Taylor expansion; therefore, this is not an acceptable solution.

4. GBT versus numerical solutions: ITG modes in tokamaks

In this section to benchmark our analytical results against the numerical solutions, we shall consider available data from the literature for a simplified fluid model of ITG modes in large aspect ratio circular tokamaks [12, 14]. To reconstruct the global mode structures with their associated global mode frequencies, local code calculations are usually performed for a range of radial flux surfaces, x, and a full 2π period in θ_0, to map out $\lambda(x,\theta_0)$. In [12, 14], for a particular equilibrium it was found that a good fit to numerical local eigenvalue data $\lambda(x,\theta_0)$, could be obtained using the form $\lambda(x,\theta_0) = \lambda_0 + \lambda_1\cos(\theta_0) + \lambda_x x + \lambda_{xx}\frac{x^2}{2}$. This model uses a Fourier expansion in θ_0 to ensure that $\lambda(x,\theta_0)$ is periodic in θ_0, and a second order Taylor expansion in x which recovers radially localised solutions in the limit $nq' \gg 1$. We note that both coefficients $\lambda_x(0,\theta_0) = \lambda_x$ and $\lambda_{xx}(0,\theta_0) = \lambda_{xx}$ are assumed to be independent of θ_0, and that only two Fourier modes are retained to model the periodic function $\lambda(0,\theta_0)$. This is the same model that we have considered in equation (17) of section 3. The best fit values of the coefficients λ_{xx}, λ_0 and λ_1 were found to be:

$$\begin{aligned}\lambda_{xx} &= 25.2200 - i31.8000\\ \lambda_0 &= -0.1183 + i0.2571\\ \lambda_1 &= 0.1257 + i0.0831.\end{aligned} \tag{52}$$

In addition, we incorporate flow shear via Doppler shift in λ_x and write

$$\begin{aligned}\lambda_{xr} &= nq'\gamma_E\\ \lambda_{xi} &= 0,\end{aligned} \tag{53}$$

where the flow shearing rate

$$\gamma_E = \frac{\mathrm{d}\Omega_\phi}{\mathrm{d}q} = \frac{1}{q'}\frac{\mathrm{d}\Omega_\phi}{\mathrm{d}x} \tag{54}$$

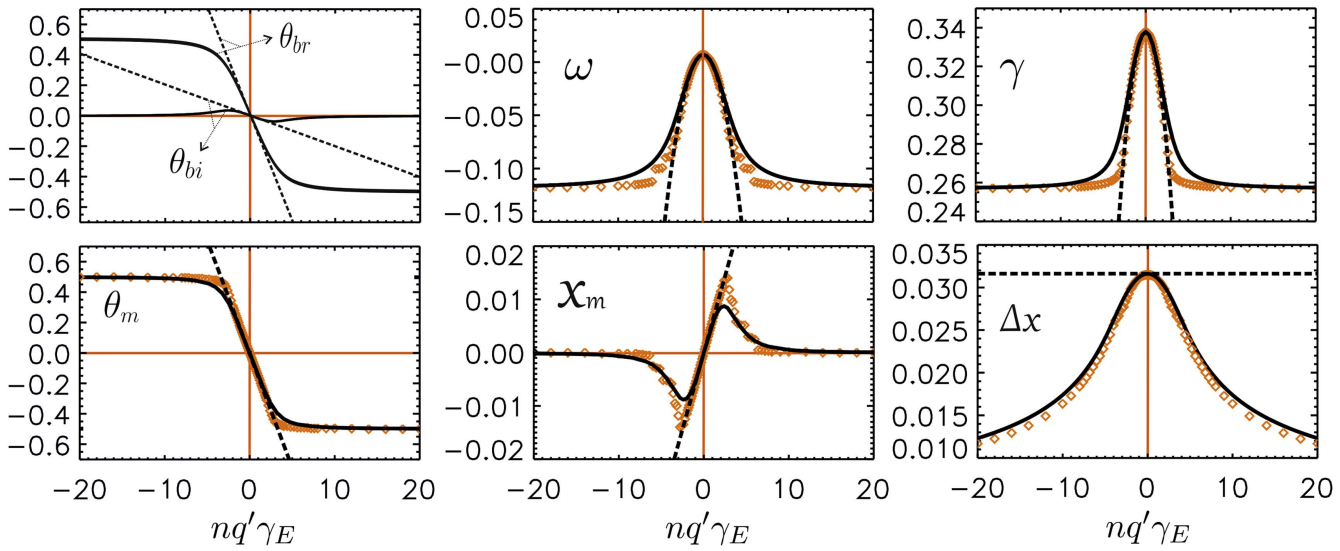

Figure 1. The global parameters; complex ballooning parameter $\theta_b = \theta_{b,r} + \mathrm{i}\theta_{b,i}$ (in units of π), global mode frequency $\Omega = \omega + \mathrm{i}\gamma$ (normalised to the electron diamagnetic frequency), the mode physical poloidal position θ_m (in units of π), the mode physical radial position x_m (normalised to the minor radius $r = 0.5$ m) and finally the mode radial width Δ_x are all plotted as a function of flow shear γ_E with $n = 50$ and $q' = 10$. Here, we have chosen $\delta = -1$ to obtain a localised mode about $\theta = \theta_m$ and sign of σ is chosen such that $\sigma = +1$ ($\sigma = -1$) for all values of $\gamma_E < 0$ ($\gamma_E > 0$). The analytical solutions are represented by solid lines while the square symbols correspond to the numerical solutions. Note that, for comparison, the WABT solutions which are indicated by dashed lines, are also presented.

is constant and Ω_ϕ is the toroidal rotational frequency of the magnetic flux surfaces with respect to the reference surface at $x = 0$. Note that, for this model, we have $[\lambda_1]_i = 0.0831 > 0$ implying, according to equation (32), that an IM on the outboard mid-plane is more unstable than an anti-IM on the inboard mid-plane. Moreover, solving equation (25) for θ_b leads to the following two solutions:

$$\theta_b^{\pm} = \sigma^{\pm}\cos^{-1}\left[-\frac{n^2q'^2\gamma_E^2}{2\lambda_1\lambda_{xx}} \pm \sqrt{\left(\frac{n^2q'^2\gamma_E^2}{2\lambda_1\lambda_{xx}}\right)^2 + 1}\right], \quad (55)$$

where in the good curvature region, corresponding to the 'minus' sign solution, as γ_E increases the mode undergoes a big radial shift with respect to $x = 0$. However, the mode in the bad curvature region, corresponding to 'plus' sign solution stays localised close to $x = 0$ for all values of γ_E. Hence, in figure 1 we only explore the 'plus' sign solutions.

Using the model coefficients from equations (52) and (53), figure 1 shows how the complex ballooning parameter θ_b, global mode frequency Ω, mode physical poloidal position θ_m, mode physical radial position x_m and the mode radial width Δ_x vary as functions of γ_E. Analytical solutions corresponding to GBT are derived in equations (20), (22)–(25) (Note that we have solved equation (25) for θ_b and the result is presented in equation (55).) while the WABT solutions are obtained from equations (34), (37), (39), (40) and(41), respectively[13]. As we can see from figure 1, for small values of flow shear corresponding to $|nq'\gamma_E| < 3.0$, both GBT solutions (solid lines) together with the WABT solutions (dashed lines), are in excellent agreement with the data obtained from the full numerical solutions of equation (2) (squared symbols). However, as flow shear increases beyond this region, the WABT solutions break down and cannot reproduce the numerical solutions. This is expected, because WABT only works for small poloidal shifts with respect to the outboard mid-plane. On the contrary, the GBT solutions correctly reproduce the numerical solutions over the full range of flow shear. Finally, in what follows, we shall only use the GBT solutions, considering an IM, MM and GM separately, and examine in detail the corresponding reconstructed global mode structures with their stability properties.

For $\gamma_E = 0$, using our GBT analytical solutions from subsection 3.1 we capture an IM for which $\theta_b = \theta_m = x_m = 0$. Furthermore, from equations (28) and (29) we obtain the analytical solutions for both the envelope $Y(\theta_0)$ and the associated global mode frequency $\Omega = 0.0070 + i0.3378$. Moreover, the reconstructed global mode structure $\tilde{\phi}(x, \theta)$ with its radial width $\Delta_x = 0.0316$ are calculated from equations (30) and (31), respectively. The corresponding numerical solutions are $\Omega = 0.0070 + i0.3378$ and $\Delta_x = 0.0316$. Here, we have solved equation (2) numerically for both $Y(\theta_0)$ and Ω and, to evaluate Δ_x, we have substituted the numerical data for $Y(\theta_0)$ into the Fourier-ballooning representation in equation (1). Numerical integration of equation (1), in turn, provides $\tilde{\phi}(x, \theta)$ and, finally, we defined Δ_x as the FWHM of a Gaussian fit to the magnitude of $\tilde{\phi}$ at $\theta = \theta_m = 0$. In figure 2, on the left-hand side, the envelope $Y(\theta_0)$ and the associated reconstructed global mode structure $\tilde{\phi}(x, \theta = \theta_m = 0)$, both the real (solid lines) and imaginary (dashed lines) components, are benchmarked against their full numerical solutions. On the right-hand side of the same figure, the colour contour plots of $\tilde{\phi}(x, \theta) = \tilde{\phi}_r(x, \theta) + \mathrm{i}\tilde{\phi}_i(x, \theta)$ in x and θ space are presented. It is quite clear that the envelope $Y(\theta_0)$ is symmetric about

[13] Note that, to obtain a localised mode about $\theta = \theta_m$ we have chosen $\delta = -1$. In addition, sign of σ is chosen such that $\sigma = +1$ and $\sigma = -1$ corresponding to $\gamma_E < 0$ and $\gamma_E > 0$, respectively.

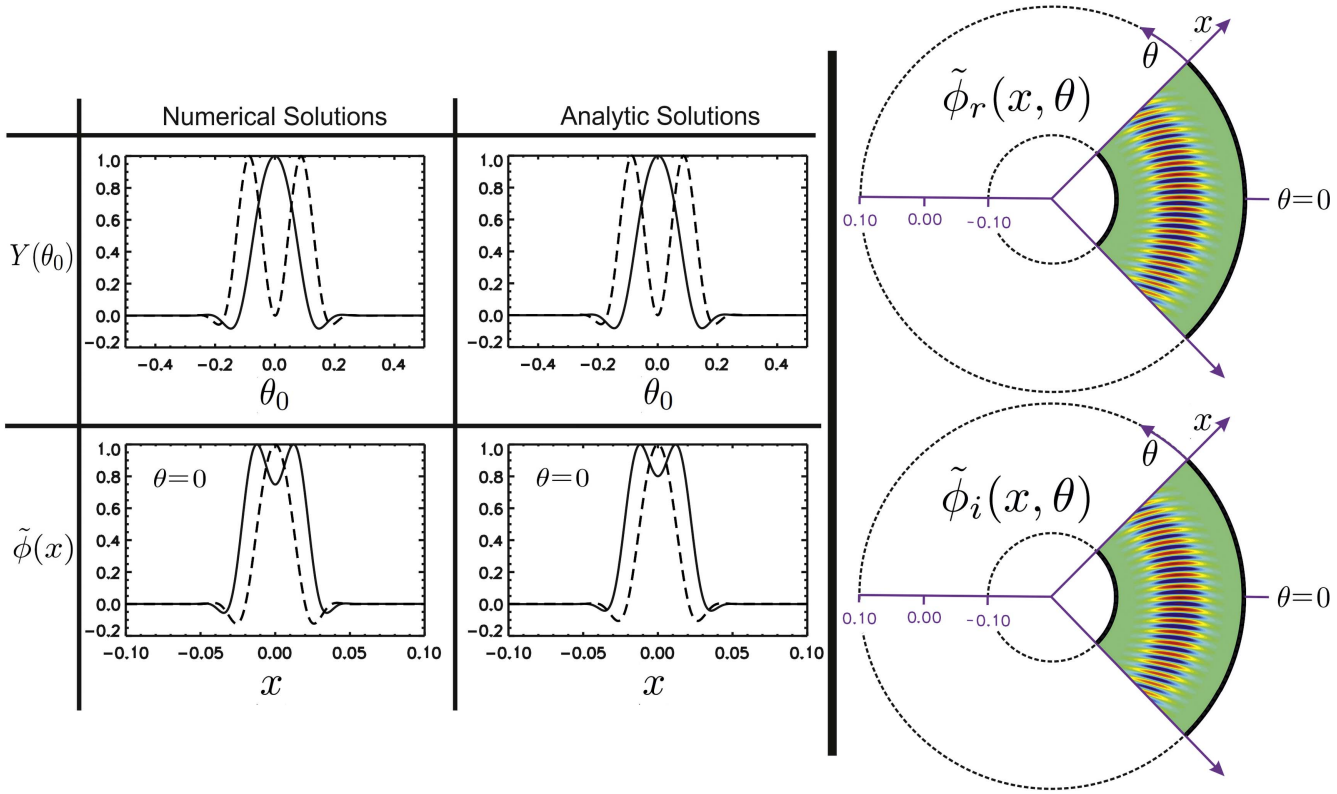

Figure 2. The envelope $Y(\theta_0)$ and the associated reconstructed global mode structure $\tilde{\phi}(x,\ \theta)$ for $nq'\gamma_E = 0$ (corresponding to an IM). [Left] Presents both analytic and numerical solutions for $Y(\theta_0)$ and $\tilde{\phi}(x,\ \theta = \theta_m = 0)$ as a function of θ_0 and x, respectively. Here, θ_0 is measured in units of π while x is normalised to the minor radius $r = 0.5$ m. Note that the solid and dashed lines correspond to the real and imaginary components, respectively. [Right] The color contour plot of $\tilde{\phi}(x,\ \theta) = \tilde{\phi}_r(x,\ \theta) + \mathrm{i}\tilde{\phi}_i(x,\ \theta)$ in the poloidal cross-section. Note that, the mode has radial symmetry.

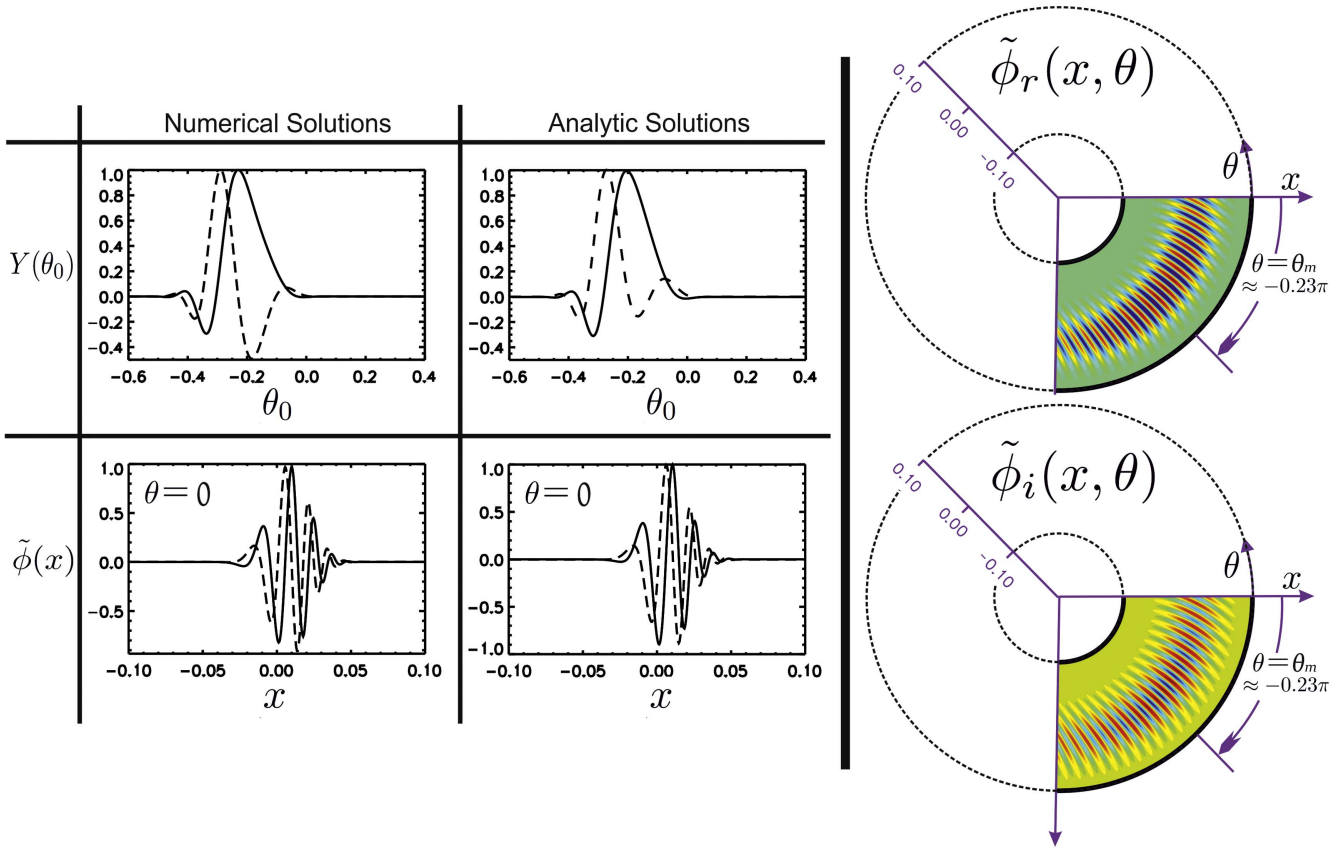

Figure 3. Equivalent set of plots to those presented in figure 2, but with $nq'\gamma_E = 1.5$ which leads to a global mode that peaks poloidally at $\theta = \theta_m \approx -0.23\pi$, rather than $\theta = \theta_m = 0$, and, in turn, has radial asymmetry.

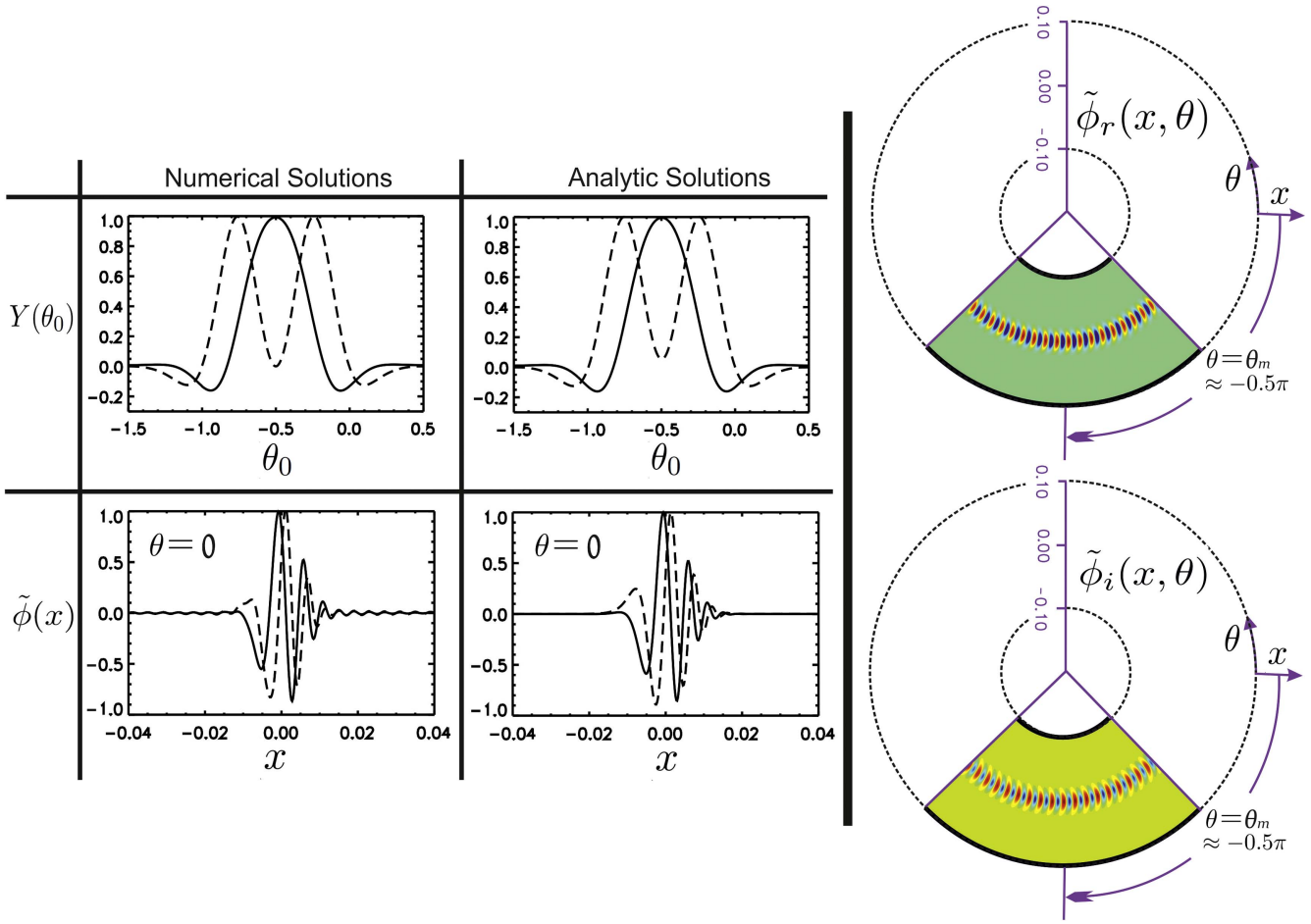

Figure 4. Equivalent set of plots to those presented in figure 2, but with $nq'\gamma_E = 20$ which leads to a general mode that sits at the bottom of the tokamak plasma, i.e. $\theta = \theta_m \approx -0.5\pi$, and, in turn, has radial asymmetry.

$\theta_0 = 0$ leading to a reconstructed global mode that peaks on the outboard mid-plane, radially centred on $x = x_m = 0$, and has a radial symmetry. This is exactly the case where $\lambda(x, \theta_0)$ has a stationary point at $x = 0$, leading to an IM that has been previously studied in [5, 10, 12] for example (see also our subsection 3.1 for more details). Finally, excellent agreement between our analytic solutions and the numerical ones are found.

Furthermore, as we switch on the flow shear the mode shifts away from the outboard mid-plane and, hence, its radial symmetry is broken. To illustrate this symmetry breaking that is associated with this class of eigenmode solutions, namely MMs, we consider an additional effect from $nq'\gamma_E = 1.5$. This corresponds to a local complex mode frequency $\lambda(x, \theta)$ that does not exhibit a stationary point on the real x axis, which in turn, according to equation (23) leads to $\theta_m = -0.224\pi$ and generates a global mode that poloidaly shifts downward with respect to the outboard mid-plane. Figure 3 shows an equivalent set of plots to those presented in figure 2, but here instead of $nq'\gamma_E = 0$ we have $nq'\gamma_E = 1.5$. The calculated complex ballooning parameter $\theta_b = -0.1907 - i0.0304$, mode radial position $x_m = 0.0086$, the mode radial width $\Delta_x = 0.0307$ and finally global mode frequency $\Omega = -0.0102 + i0.3160$ are obtained from equations (25) (or equivalently equation (55)), (24), (22) and (20), respectively. The corresponding numerical solutions are $\theta_m = -0.230\pi$, $x_m = 0.0087$, $\Delta_x = 0.0307$ and $\Omega = -0.0104 + i0.3162$, respectively. Moreover, the envelope $Y(\theta_0)$ is not symmetric about $\theta_0 = \theta_m = -0.23\pi$ (corresponds to $\theta_{bi} = -0.0304 \neq 0$) and this is the source of the above observed radial shift ($x_m \neq 0$). In addition, because $\theta_m \neq 0$, the reconstructed global mode structure is not radially symmetric about $x = x_m$. We also point out that in this region, corresponding to the intermediate values of flow shear, a slight discrepancy between our GBT results and numerical solutions are observed. This might be attributed to the fact that we have only retained the first two terms when we Taylor expanded equation (2) about $\theta_0 = \theta_b$.

Finally, as we can see for large values of flow shear, $nq'\gamma_E \gg 1$, the global parameters in figure 1 approach constant values. For this limit, considering $nq'\gamma_E = 20$, figure 4 shows the envelope $Y(\theta_0)$ together with the corresponding reconstructed global mode structure $\tilde{\phi}(x, \theta)$. Here, to obtain the numerical solutions we have solved equations (1) and (2) numerically, while the corresponding analytic solutions for $Y(\theta_0)$ and $\tilde{\phi}(x, \theta)$ are given by equations (19) and (21) (or equivalentlys equations (48) and (49)), respectively. Note that, due to the fact that $Y(\theta_0)$ is symmetric about $\theta_0 = -\pi/2$, corresponding to $\theta_{bi} = 0$, $\tilde{\phi}(x, \theta)$, in turn, is centred on $x = 0$.

We can see that the radial slice from the constructed eigenmode structure is not symmetric on the outboard mid-plane at $\theta = 0$. Moreover, the analytic solutions for $\Omega = -0.1183 + i0.2571$ and $\Delta_x = 0.0122$ are obtained from equations (20) and (22) (or equivalently equations (46) and (50)), respectively, and their corresponding numerical solutions are $\Omega = -0.1179 + i0.2571$ and $\Delta_x = 0.0117$. Finally, it is worth mentioning that, good agreement is again found between analytical and numerical solutions.

5. Summary and conclusions

In the context of higher order ballooning theory, we have developed a new analytical approach, namely GBT, to account for a global mode that balloons at arbitrary poloidal position with respect to the outboard (or inboard) mid-plane of tokamak plasmas. The so-called WABT, which only provides accurate results for a mode that sits close to the outboard mid-plane, is recaptured as a special limit from our GBT theory. Furthermore, to benchmark GBT against the numerical solutions, we have used available data from a simplified fluid model for the toroidal linear electrostatic ITG modes in circular tokamaks. It is found that the parameter regimes with moderate and large poloidal shifts, corresponding to $|\gamma_E| > 3$ in figure 1, cannot be covered in the context of WABT treatment, but GBT works well in this region. Specifically, the inter-mode transition between IM and GM can only be captured in the context of our GBT theory.

Moreover, it is shown that the imaginary component of the ballooning parameter θ_b leads to a mode that radially shifts away from its associated rational surface at $x = 0$. In addition, our theory has revealed that the IMs are the only modes that preserve radial symmetry. The radial asymmetry that is associated with the non IMs, caused by profile shearing, can be used, in the context of GBT, as an important tool to investigate the mechanism that generates the so-called Reynolds stress.

Furthermore, GBT is a quite general theory which can be employed and combined with a state-of-art local gyrokinetic code, GS2, GKW, GENE and GYRO for instance, to improve our understanding of the linear microinstabilities for realistic experimental regimes. Unlike previous ballooning treatments, our theory can be applied to experimentally relevant equilibria for which the shape of magnetic flux surfaces are not, in general, circular and one usually needs to consider the effect of radial profile variations. On the other hand, it is worth mentioning that our GBT theory, as with previous ballooning treatments, has the following limitations: (a) equation (2) is derived under the assumption that equilibrium quantities vary slowly across rational surfaces, (b) the approach only works in linear regimes. It will be interesting to consider whether this approach can be extended to the nonlinear regimes, but this is quite challenging and it is not clear yet how to achieve this. Nonetheless, the linear instabilities with their mode structures remain interesting; for example, quasi-linear theory, frequently used to model the transport that is associated with microturbulence, assumes that the saturated nonlinear mode structure continues to resemble the linear mode.

Finally, the approach outlined in this paper obtains the mode amplitude envelope to leading order in $1/n$ by solving equation (2). This amplitude envelope captures the leading order impact of equilibrium profile variation on the radial localisation of the linear mode structure, which is an important physical fluctuation property that requires solving the gyrokinetic equation over a radially extended domain. We note that this method does not capture $O(1/n)$ corrections to the fluctuations, which requires a considerably more sophisticated treatment that includes the neoclassical equilibrium corrections.

Acknowledgments

P A Abdoul appreciate the financial support by the Ministry of Higher Education in Kurdistan region of Iraq. This work has been (part-) funded by the RCUK Energy Programme [grant number EP/P012450/1]. The authors acknowledge helpful discussions with J W Connor.

ORCID iDs

P A Abdoul https://orcid.org/0000-0002-2144-8336
H R Wilson https://orcid.org/0000-0003-3333-7470

References

[1] Horton W 1999 *Rev. Mod. Phys.* **71** 1–8
[2] Abdoul P, Dickinson D, Roach C M and Willson H R 2015 *Plasma Phys. Control. Fusion* **57** 065004
[3] Camenen Y, Idomura Y, Jolliet S and Peeters A G 2011 *Nucl. Fusion* **51** 1–11
[4] Hill P, Saarelma S, McMillan B, Peeters A and Verwichte E 2012 *Plasma Phys. Control. Fusion* **54** 1–8
[5] Connor J W, Hastie R J and Taylor J B 1978 *Phys. Rev. Lett.* **40** 396
[6] Connor J W, Hastie R J and Taylor J B 1979 *Proc. R. Soc.* A **365** 1
[7] Hastie R J, Hesketh K W and Taylor J B 1979 *Nucl. Fusion* **19** 1223
[8] Pegoraro F and Schep T 1981 *Phys. Fluids* **24** 478
[9] Connor J W, Taylor J B and Wilson H R 1993 *Phys. Rev. Lett.* **70** 12
[10] Taylor J B, Wilson H R and Connor J W 1996 *Plasma Phys. Control. Fusion* **38** 243–50
[11] Xie T, Zhang Y Z, Mahajan S M and Wang A K 2012 *Phys. Plasmas* **19** 072105
[12] Dickinson D, Roach C M, Skipp J M and Wilson H R 2014 *Phys. Plasmas* **21** 010702
[13] Abdoul P 2015 *PhD Thesis* (http://etheses.whiterose.ac.uk/10011/)
[14] Dickinson D 2012 *PhD Thesis* (http://etheses.whiterose.ac.uk/3331/)
[15] Zhang Y Z and Mahajan S M 1991 *Phys. Lett.* A **157** 133
[16] Xie T, Qin H, Zhang Y Z and Mahajan S M 2016 *Phys. Plasmas* **213** 042514

[17] Bokshi A, Dickinson D, Roach C M and Wilson H R 2016 *Plasma Phys. Control. Fusion* **58** 075011
[18] Connor J W and Martin T J 2007 *Plasma Phys. Control. Fusion* **49** 1497–507
[19] Terry P W 2000 *Rev. Mod. Phys.* **72** 109–65
[20] Kishimoto Y *et al* 1999 *Plasma Phys. Control. Fusion* **41** 3A
[21] Roach C M *et al* 2009 *Plasma Phys. Control. Fusion* **51** 124020
[22] Biglari H, Diamond P H and Terry P W 1990 *Phys. Fluids* B **2** 1–4
[23] Waltz R E, Kerbel G D and Milovich J 1994 *Phys. Plasmas* **1** 2229–44
[24] Xie T, Zhang Y Z, Mahajan S M, Liu Z Y and He H 2016 *Phys. Plasmas* **23** 102313
[25] Zhang Y Z, Mahajan S M and Zhang X D 1992 *Phys. Fluids* B **4** 2729–32
[26] Lu Z X, Fable E, Hornsby W A, Angioni C, Bottino A, Lauber P and Zonca F 2017 *Phys. Plasmas* **24** 042502
[27] Zhang Y Z and Mahajan S M 1995 *Phys. Plasmas* **2** 4236
[28] Burrell K 1997 *Phys. Plasmas* **4** 1499
[29] Kneser H 1958 *Funktionentheorie* (Göttingen: Vandenhoeck und Ruprecht) p 121
[30] Remmert R 1958 *Theory of Complex Functions* (New York: Springer) pp 413–4